

## BOND GFRP-CONCRETE UNDER ENVIRONMENTAL EXPOSURE

Hugo Biscaia<sup>\*</sup>, Manuel A. G. Silva<sup>\*</sup> and Carlos Chastre<sup>\*</sup>

<sup>\*</sup> UNIC Research Center/ Faculdade de Ciências e Tecnologia / Universidade Nova de Lisboa  
2829-516 Caparica, Portugal  
e-mail: @fct.unl.pt, web page: <http://www.dec.fct.unl.pt>

**Key words:** Durability, glass fiber composites, bond, concrete.

**Summary.** *Fiber reinforced polymers (FRP) are often used to strengthen RC structures. Despite intense research, durability of reinforced concrete (RC) retrofitted with FRP remains insufficiently known. Long time behavior of the bond laminate-concrete, in flexural strengthening, under environmental action is not well known, conditioning Codes and engineers. An experimental program that subjected RC beams, externally reinforced with Glass FRP (GFRP) strips, to temperature and salt water cycles, for up to 10000h is reported. At selected intermediate times, the RC beams were loaded to failure in bending. Rupture took place, normally, by tensile failure of concrete at a short distance from the interface with GFRP. The results showed that freeze-thaw cycles were the most severe of the environmental conditions. The study also generated also non-linear bond-slip relationships from the experimental data. Numerical modeling has been undertaken, based on a commercial code. The model is based on smeared cracking. Parameters needed for the characterization, namely cohesion and friction angle, were obtained from shear tests conceived for the effect.*

### 1 INTRODUCTION

The strengthening of structural elements of reinforced concrete with FRP composites has been emerging as a method with great potential to increase the resistance of RC elements. However, the life span of structures has become important public concern and more data are needed on degradation of structures externally reinforced with FRP. The diffusion of OH<sup>-</sup> and Cl<sup>-</sup> ions and water into the polymeric matrix, causes hydrolysis and depolymerization and may be present due to de-icing and moisture rising from foundations, for example, decreasing tensile strength and stiffness. Additionally, external strengthening with FRP depends on bond between concrete and laminate [1], with failure occurring often near the surface of adherence. Publications on the behavior of FRP reinforced members subjected to environmental effects exist, but known data are still insufficient. Numerical modelling has been described by several authors based on assumed failure mechanisms and different computational approaches [e.g. 2, 3, 4 and 5] showing results in good agreement with experimental tests.

The mechanism of the bond between the FRP and concrete is affected by several variables, including the geometry of the FRP strips, the concrete and the adhesive. Studies that aim to simulate a possible premature debonding between the FRP and concrete based on

the energy of fracture are consistent and provide good estimations of the opening of cracks on the basis of two criteria of fracture modes: Mode I and Mode II [2]. In this study an analysis with both methods was considered utilizing ATENA computer code.

The modelling of the bond GFRP/concrete was based on a finite element interface using the theory of Mohr-Coulomb rupture. Cohesion and friction angle were obtained experimentally. Other parameters such as normal and tangential stiffness were considered equal to, respectively,  $3 \times 10^8$  MN/m<sup>3</sup> and  $3 \times 10^4$  MN/m<sup>3</sup> based on experimental testing of reinforced concrete beams subjected to bending [6].

## 2 MATERIALS CHARACTERIZATION

### 2.1 Concrete

Concrete cubes at 28 days had an average compressive strength of 34.9 MPa. Table 1 presents a summary of the characterization of concrete at 28 days.

$f_{cm,cub}$ (MPa)	$f_{cm}$ (MPa)	$f_{ctm}^*$ (MPa)	$E_{cm}^*$ (GPa)
43.58	34.87	2.69	32.00

Table 1: Characterization of the concrete at 28 days.  
\* Values based on correlations of EC2 [7].

Given that all samples are from the same concrete, the development of compressive resistance of concrete,  $f_c$ , versus time,  $t$ , was obtained by regression analysis using the results of the cubic compression tests leading to

$$f_c(t) = 30.852 \cdot t^{0.036}, \quad t \text{ in days} \quad (1)$$

From this equation, it appears that the increase of compressive strength had no significant influence on the final results.

### 2.2 GFRP laminates

Unidirectional GFRP laminates 2.54 mm thick (2 layers of 1.27 mm for each layer) were used and tensile tests performed on flat coupons. The speed of the test was 2 mm/min and the remaining procedures of the tests were conducted according to ASTM D3039 / D 3039M.

The flat coupons tested have a linear elastic behavior until failure with an average rupture tension of 500.2 MPa and average strain of 2.46%. The Young modulus obtained was 20.39 GPa.

Epoxy resin Tyfo® S was used as adhesive between GFRP and concrete as was used in the impregnation of glass fibers. Table 2 sets out some mechanical characteristics of the resin provided by the manufacturer where  $\sigma_r$  is the rupture tensile stress,  $\varepsilon_r$  is the rupture strain and  $E_r$  is the Young modulus.

Properties	Standard	Typical tests values
$\sigma_r$	ASTM	72.4 MPa
$E_r$	D-638	3.18 GPa
$\epsilon_r$	Type 1	5.0%

Table 2: Mechanical characteristics of the resin.

### 3 EXPERIMENTAL STUDY

#### 3.1 Artificial aging tests

Artificial aging was imposed corresponding to total immersion in salt water, temperature cycles, salt fog cycles and wet/dry cycles. Salt fog cycles were imposed with the same salinity (50 g/l water) as immersion, keeping temperature in the vicinity of 35°C and 16h drying, followed by 8h of fog. Temperature cycles imposed -10°C for 12h, followed by +10°C for another 12h. Each 24h cycle is represented in Fig. 5. Finally, each wet/dry cycle consisted of 3 days of total immersion in 5% of salt water followed by 4 days of drying.

The specimens were tested after 1000, 5000 and 10000 hours of exposure. At the beginning of artificial aging (0 hours of exposure) tests were made to compare results with those obtained at the times indicated above and the average of the corresponding results are referred in the sequel as reference values [6].

At the start of the artificial ageing, the composite reinforcement had been bonded to the concrete (and curing) for 60 days in the case of salt fog, wet dry cycles and immersion in salt water and 48 days in the case of temperature cycles.

#### 3.2 Bending tests

Each tested specimen consisted of two independent blocks of reinforced concrete (300×150×100 mm<sup>3</sup> each block) Figure 1, with tops connected by a metal hinge. The two low surfaces of the RC blocks were connected by a 520 mm long and 80 mm wide strip of two layers GFRP reinforcement at the base level. The GFRP composite was applied by the wet lay up technique. When load was applied to the beam, the GFRP was tensioned, subsequently transmitting shear stresses to the concrete.

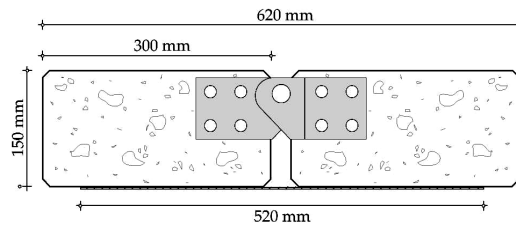


Figure 1: Geometry of the specimens to be submitted to bending tests.

The bond length of GFRP in each block was 240 mm. Using different suggested expressions [8, 9, 10 and 11] for determining the effective bond length it was concluded that the values obtained were lower than the bond length used on this study. Therefore, the bond

length used on the specimens was sufficient to mobilize the maximum strength of the GFRP/concrete bonding.

The load was applied through an actuator supported against a steel frame as shown in Figure 2. The control of the applied load was made by two load cells placed under the supports of the specimen. The specimens were instrumented with strain gauges bonded to the GFRP strip, spaced at intervals of 40 mm to measure the strain distribution along the GFRP laminate at different loading levels (see Figure 3). A displacement transducer was used to measure the vertical displacement at the specimen mid-span. A HBM data-logger was used in order to collect data from load cells, strain gauges and the displacement transducer.

From the measurements taken along the reinforcement of GFRP it was found that during the test the maximum shear stress between GFRP and concrete began to occur in the central area of the beam. For loads that are closer to the rupture load the shear stresses tend to be spread along the length of bonding, and distributed in a more uniform way. This feature is agreement with the *fib* bulletin 14 for bond between concrete and CFRP with a thickness of 1.2 mm and a bond length of 50 mm x 250 mm wide. Similar conditions can be found in another study with CFRP under circumstances similar to those studied in this work [12].



Figure 2: Bottom view of location of strain gauges in bending tests.



Figure 3: Overview of the standard bending test scheme.

The axial stresses in GFRP are low and symmetrical for low load levels. As the vertical load is increased, the axial stress in the GFRP also increases, but in a more non symmetrical way. Near the end of the GFRP strip, these stresses do not develop significantly with the load increases.

The shear stresses,  $\tau_{sh}$ , may be positive or negative depending on the development of axial stresses in the GFRP growing or decreasing along the bonding length. The negative shear stress in the FRP can be justified by the appearance of cracks in concrete. When the axial stresses,  $\sigma$ , in the FRP or forces,  $F$ , in the FRP remain constant in consecutive strain gauge readings, it means that the shear stresses take a null value, which can be translated by the debonding of the FRP [13], as shown in Figure 4. Given the linear behavior of the FRP, the shear stress can be calculated from Equation 2 [13] where  $\tau_{sh}$  is the stress in the fiber,  $t_f$  is the thickness of the fiber,  $\Delta\epsilon$  is the fiber strain differential between consecutive gauges and  $\Delta L$  is the distance between consecutive strain gauges.

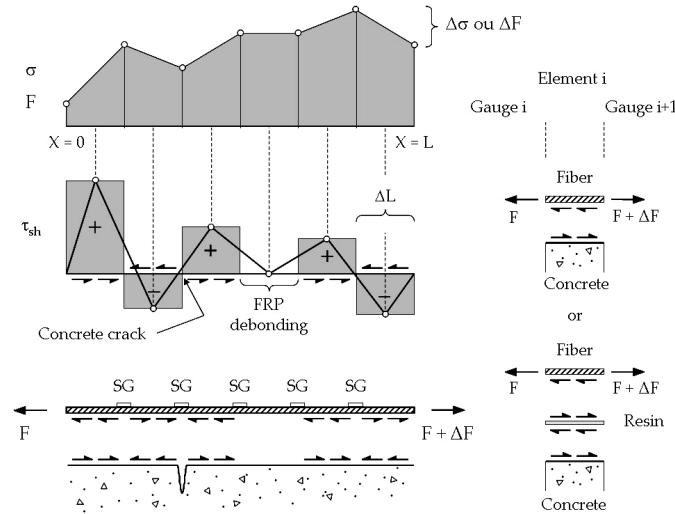


Figure 4: Development of shear and axial stresses in a bond between FRP and concrete. Based on [13].

$$\tau_{sh} = \frac{\Delta \varepsilon \cdot E_f \cdot t_f}{\Delta L} \quad (2)$$

As shown in Figure 5, the reference specimens reached a very similar rupture load, whereas for the specimen GR-REF-1 the rupture load was slightly higher ( $P_{max} = 29.85$  kN). Specimen GR-REF-4 showed the highest mid span displacement ( $\delta_{max} = 3.2$  mm).

The failure of reference specimens was due to concrete tensile failure in the concrete near the surface and concrete could be seen adherent to the GFRP strips after rupture. Typical post-failure configurations are represented in Figure 5.



Figure 5: Post-failure surface of the reference specimens.

Bond slip was found by integration of the strains measured from strain gauges along the GFRP reinforcement. A typical set of curves is shown in Figures 6 and 7. Figure 7 shows the distribution of axial stresses on GFRP, along the beam, for different load intensities, for a beam that had been subjected to 5000h of salt fogging. Immersion in salt water showed a gain of 21% on the capacity of beams at 10000h due to the conjugated effect of strength increase of concrete and post-curing of resin.

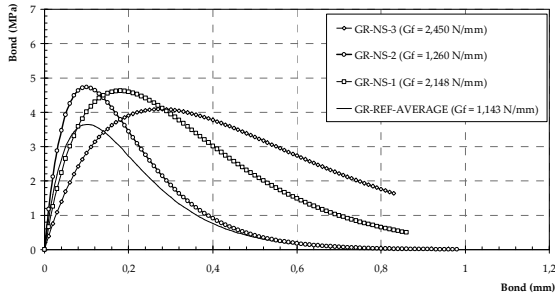


Figure 6: Comparison between the bond-slip laws obtained from the salt fog bending tests and the average bond-slip law without ageing.

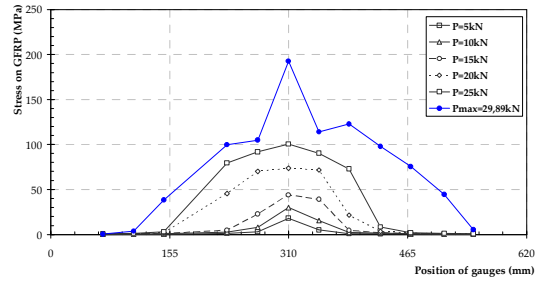


Figure 7: Typical stress diagram as loading of specimen increases (case of salt fog – 5000 h).

In the case of salt fog cycles, immersion in salt water and wet/dry cycles failure occurred with separation of the GFRP strip close to the interface with concrete, as shown in Figure 8, and the average bond stress was always greater than in the reference specimens without aging (0 hours). This fact might explain the more irregular distribution and lower bond stress encountered in the specimens tested prior to aging or submitted to temperature cycles.

The force in the laminate for the beams subjected to total immersion increased about 21%, and decreased 31% in the case of temperature cycles. Failure loads after temperature cycles were increasingly reduced. Total immersion improved the strength, leading to higher values of the ultimate load that reached an increase of 20% at 10000 hours [14].

### 3.3 Shear tests

In order to model numerically the nonlinear behavior of the bond between GFRP and concrete, shear tests were performed to obtain the necessary data. ATENA can model bond between two elements using interface finite elements based on the Mohr-Coulomb criteria and requires cohesion,  $c$ , and internal friction angle,  $\varphi$ , of the adhesion between GFRP and concrete.

The tests were based on 15 cm wide concrete cubes, with two-layered GFRP laminates of 8 cm width glued to both sides of the cubes with an average anchor length of 14 cm, Figure 8. Tests were carried out with no lateral compression (mc1: simple shear test), and with lateral compression,  $\sigma_{comp}$ , equal to 0.5 MPa (mc-4), 1.0 MPa (mc-3) and 2.0 MPa (mc-2). The results obtained on these tests are shown in Table 3. The internal friction angle ( $\varphi$ ) of the bond was obtained from Equation 3 [15].

Figure 9 shows the force-displacement curves of bond between GFRP and concrete corresponding to the shear tests with and without lateral compression.

$$\tau = c + \varphi \cdot \sigma \quad (3)$$



Figure 8: Shear test apparatus.

Test (MPa)	$\sigma_{comp}$ (MPa)	$\tau_{ader}$ (MPa)	$\varphi$	$\delta_{max}$ (mm)
mc-1	0	2.60	0	2.25
mc-2	2.01	5.20	1.28	6.11
mc-3	0.99	4.69	2.04	4.49
mc-4	0.50	3.69	2.24	3.56

Table 3: Shear tests for characterization of Mohr Coulomb type of failure.

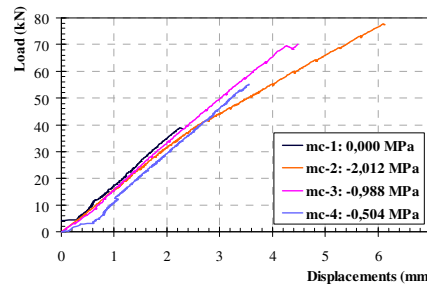


Figure 8: Force-displacement graph of the shear tests with and without lateral compression.

#### 4 NUMERICAL MODELLING

The analyses were carried out using commercial code ATENA. The constitutive model of concrete includes non-linear behavior in compression; fracture of concrete in tension based on the nonlinear fracture mechanics; biaxial strength failure criterion; reduction of compressive strength after cracking; tension stiffening effect; reduction of the shear stiffness after cracking (variable shear retention); two crack models: fixed crack direction and rotated crack direction [15].

Perfect bond between concrete and steel rods was assumed. Steel was assumed to have elasto-plastic behavior with a Young modulus of 210 GPa and yield stress of 210 MPa. GFRP reinforcement was assumed to have a linear behavior until rupture with a Young modulus of 20.39 GPa.

Quasi-brittle materials such as concrete do not exhaust the tension strength after a stress equal to the tension strength. The ruin of a FRP-concrete interface is, commonly, in the concrete substrate so the crack growing in these interfaces can be described as: (1) the uncracked zone, where the interface has not been loaded up to the interface strength; (2) the microcracked zone, where the interface and the concrete layer near the interface began to microcrack due to the load increase; and (3) true crack, where there isn't no shear stress transmission through the interface. The tensile crack model for Mode I behavior and the sliding crack model for Model II behavior are reproduced by the softening curve for the normal and shear strength crack, as shown in Figure 9.

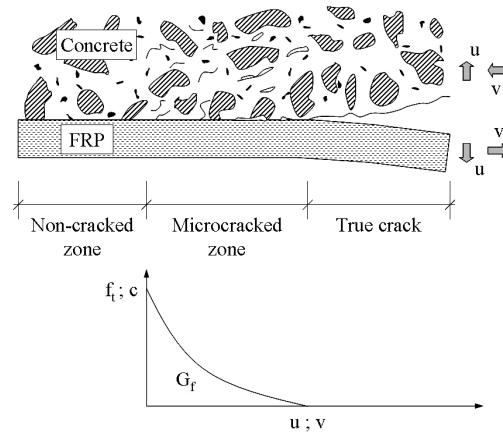


Figure 9: Cracking process in the FRP-concrete interface and profile of the softening laws

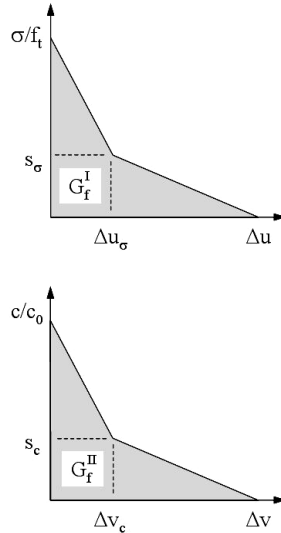


Figure 10: Example of a softening law for tension and cohesion.

Isolating these two modes it is possible to define the softening laws for tensile as well as shear softening. In [15] softening laws are proposed, being their break points determined by Equations 4.

$$u = \frac{f_t}{4} \quad (4.a)$$

$$v = 0.75 \times \frac{G_f}{f_t} \quad (4.b)$$

The constitutive relations that were considered during this study were based on the experimental work of [6], except for softening law tension in which it was admitted that the fracture energy for Mode II was ten times the fracture energy for Mode I [16]. Thus, the necessary values to correctly define these softening laws were:  $\Delta u_{\sigma} = 0.024$  mm;  $\Delta u = 0.157$  mm;  $s_{\sigma} = 0.25$ ;  $\Delta v_c = 0.236$  mm;  $\Delta v = 0.583$  mm; and  $s_c = 0.25$ .

#### 4.1 Bending models

The finite element mesh was automatically generated with triangular and rectangular finite elements with about 10 mm, refined down to 2 mm near the interface between GFRP and concrete. The loading was simulated by vertical deflection increments of 0.02 mm, applied at load points used in the experimental tests representing the application of the quasi-static applied load. A similar criterion was also adopted for the simulation of shear tests. Figure 12 shows the deformed models increased 5 times with the finite element mesh considered for both tests as well as the concrete cracking.

The numerical study of the bending specimens revealed that the maximum force achieved was up to 26.8 kN and it also allowed to notice that: (1) on concrete, the maximum compressions occurs near the hinge and caused a stress of 24.9 MPa (lower than concrete compression stress); (2) on GFRP, the maximum stress was 130.8 MPa (lower than the tensile strength of GFRP) at the free end of the GFRP, so this wasn't the rupture mechanism of the beam; and (3) on resin, the maximum stress in the model never reached the tensile strength of 72.4 MPa, so the rupture was not by the resin either.

The interface envelope curve is represented in Figure 11. No point outside the envelope curve satisfies the rupture law, so it means that debonding occurred. In Figure 12, the force-stress law may be useful to identify the force that corresponds to the initial crack opening at the strain gauges position.

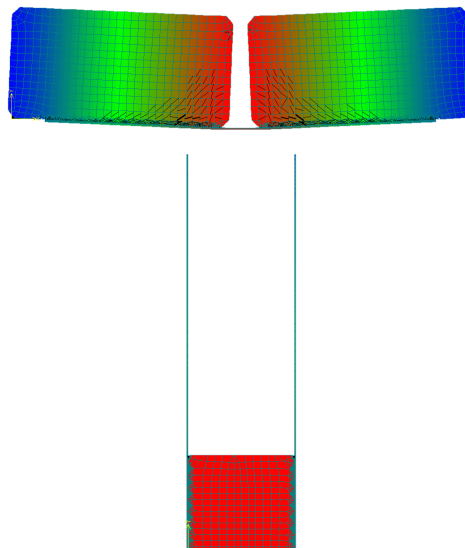


Figure 11: Deformed models with finite element mesh – bending model (top) and shear model (bottom).

Comparing the numerical analysis with the experimental tests, the results were quite reasonable with the exception of the value of the shear stress with a maximum error of 31.2% as shown in Table 4.

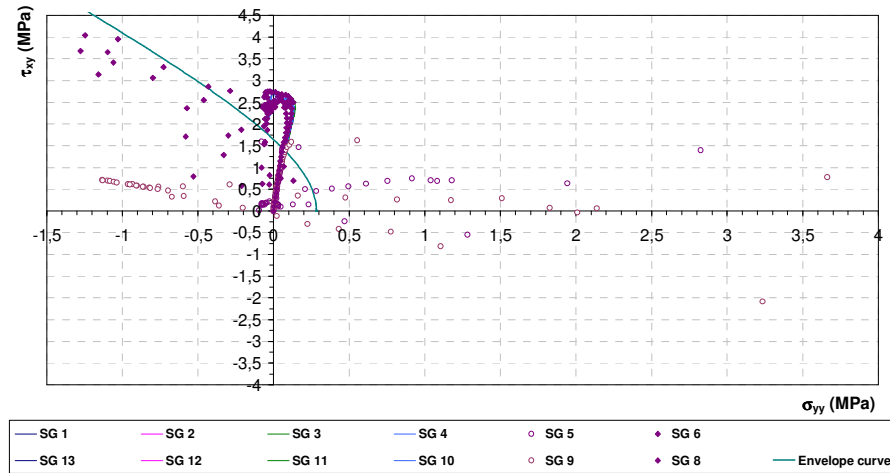


Figure 12: Envelope curve of the reference beam specimens.

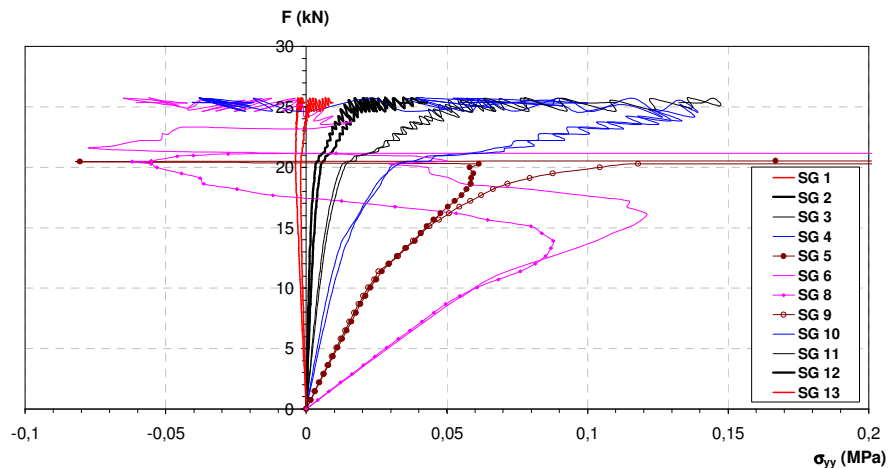


Figure 13: Force-stress graph for identification of the crack opening position.

## 4.2 Shear models

Experimental shear tests conducted to the force-displacement curves that are presented in Figure 13. It can be noted that the bond stiffness between GFRP and concrete had an almost linear behavior, except for the specimen with a compressive stress of 2.0 MPa. The maximum response in this sample was 77.6 kN. However, assuming a linear response, the expected value would be approximately 100 kN, in other words, an increase of 0.5 MPa in the compressive stress leads to an increase of approximately 15 kN in the maximum force,  $F_{max}$ .

Figure 13 shows that the maximum force on bond has proved to be a parameter obtained with exceptional accuracy. Model mc-3 showed lowest error for maximum displacement

(2.57%). In Table 5, it can be observed that the specimen mc-4 had the lowest error (8.04%) at the maximum GFRP strain.

Average exp. values	ATENA	Error
Maximum force (kN)		
28.1	26.79	5.06%
Force on GFRP (kN)		
25.4	24.37	4.2%
Maximum shear stress (MPa)		
3.7	2.82	31.2%
Maximum strain (%)		
0.60	0.588	1.5%
Maximum normal stress (MPa)		
121.8	119.95	1.5%

Table 4: Comparison between the values obtained experimentally and the values obtained by ATENA.

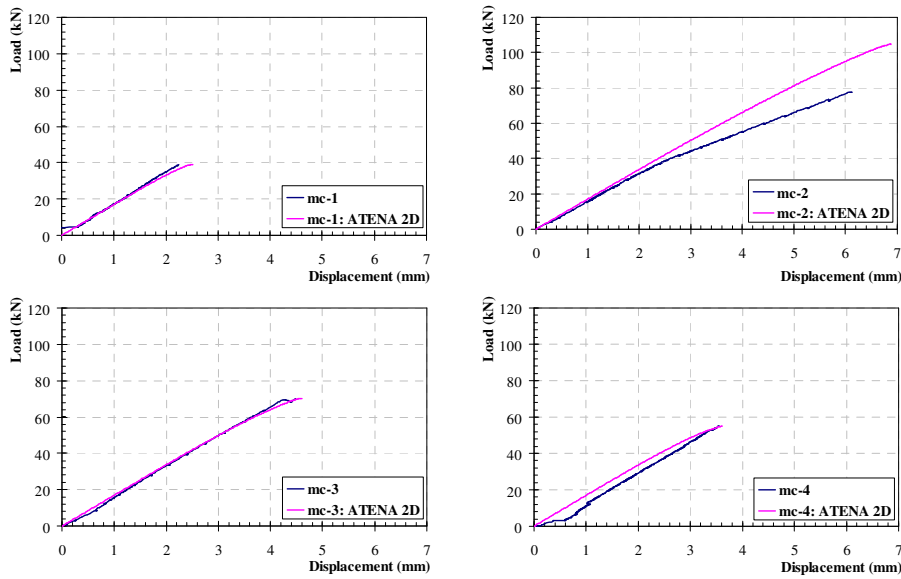


Figure 13: Force-displacement graph of the shear numerical models compared to that obtained experimentally.

	Average exp. values (%)	ATENA (%)	Error
mc-1*	-	-	-
mc-2	0.85	1.28	33.59%
mc-3	0.76	0.86	11.60%
mc-4	0.63	0.68	8.04%

\* There were no readings of the strain gauges.

Table 5 – Comparison of the maximum strain on GFRP.

### 4.3 Parametric study

In order to define precisely bond between GFRP and concrete, it is imperative to know the right values for cohesion and internal friction angle. Therefore, it is expectable that a refined interface finite element will lead to a better design of these environmental effects. In order to improve the understanding of the effects of these properties on aging models, results are presented for two situations: (1) fixing cohesion and varying the internal friction angle; and (2) fixing the internal friction angle and varying cohesion (see Figures 14 and 15).

In this analysis it was observed that the shear stress tend do increase with cohesion. For instance, when cohesion is 4.0 MPa the shear stress developed in the model was 4.81 MPa and when cohesion is 1.0 MPa the shear stress developed was only 1.45 MPa. When cohesion is fixed, it was observed that the shear stress become more affected for higher internal friction angle, for instance, only when internal friction angle turn out to be 5.67, the shear stress developed reached 5.21 MPa, until then, shear stress oscillate between 2.80MPa and 3.34 MPa.

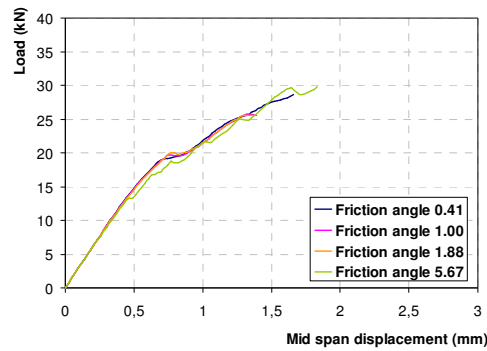


Figure 14: Force-displacement graph for fixed cohesion.

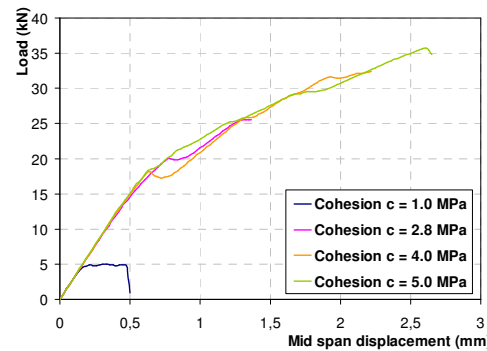


Figure 15: Force-displacement graph for fixed internal friction angle.

## 5 CONCLUSIONS

It was possible to model the interface between GFRP and concrete based on Mohr-Coulomb rupture theory using the shear tests here proposed as well as obtain the values of cohesion and internal friction angle of the bond GFRP/concrete. Based on these values, the

modelling of the bond between GFRP and concrete has proved to be acceptable.

Modelling of the shear tests proved to be more precise than the modelling of the bending tests, especially the value for the maximum load (except model mc-2). The level of strains in the GFRP obtained from the numerical models had errors ranging from 1.5% to 11.6% (except in model mc-2).

The maximum shear stresses in the bond GFRP/concrete obtained by experimental tests revealed some disagreement with those obtained by computational analysis, in spite of a reasonable qualitative similarity of the development of shear stresses over the anchor length.

In the beam model, the rupture stress of the GFRP or the resin were never reached at the time of rupture, which took place where the concrete cracks appeared in the same direction during the experimental tests. Equal evidence happened in the shear specimens, but in these cases the cracking was less obvious in terms of the experiments or in the ATENA model.

Based in the results, it seems appropriate for these materials in the GFRP/concrete interface (without environmental aging) to be simulated by a cohesion value of 2.8 MPa and an internal friction angle of  $62^\circ$ .

More experimental tests are being made in order to assess the bond behaviour when affected by different environmental aging. Meanwhile, it is of high importance to understand the evolution of the phenomena if simultaneous variation on cohesion and internal friction angle takes place as a result of the degradation imposed by aging.

The parametric study permitted to conclude that cohesion is a parameter that has huge influence on the final results of the modelling while internal friction seems to be more influence for high values. Therefore, the right characterization of these parameters is an issue that has a huge importance during the modelling of an external reinforcement with FRP.

## REFERENCES

- [1] Silva, Manuel A.G., Biscaia, H., *Degradation of bond between FRP and RC Beams*, Composite Structures, vol. 85, Issue 2, pp.166-174.
- [2] Pham, H.B.; Al-Mahaidi, R. e Saouma, V., *Modelling of CFRP-concrete bond using smeared and discrete cracks*, Composite Structures, 2006.
- [3] Sena Cruz, J.M.; Barros, J.A.O.; Gettu, R. e Azevedo, A.F.M., *Bond behaviour of near-surface mounted CFRP laminate strips under monotonic and cyclic loading*, Journal of Composite for Construction, ASCE, 2006, pp. 296-303.
- [4] Camata, G.; Spacone, E. e Zarnic, R., *Experimental and nonlinear finite element studies of RC beams strengthened with FRP plates*, Composites Part B: engineering, 2006.
- [5] Neale, K.W.; Ebead, U.A.; Abdel Maky, H.M.; Elsayed, W.E. e Godat, A., *Modelling of debonding phenomena in FRP-strengthened concrete beams and slabs*, International Institute for FRP in Construction, 2005.
- [6] Biscaia, H.E.C., *Rotura por perda de aderência entre reforços poliméricos com fibras de vidro e elementos estruturais de betão*, Dissertation to obtain the Master degree in Civil Engineering – Engineering of Structures orientation, Instituto Superior Técnico, Universidade Técnica de Lisboa, 2006.
- [7] Eurocode 2 (EC2), *Eurocode 2: Design of concrete structures - Part 1-1: General rules*

- and rules for buildings*, EN 1992-1-1, December 2004.
- [8] Teng, J.G.; Chen, J.F.; Smith, S.T. e Lam, L., *FRP strengthened RC structures*, John Wiley and Sons Ltd. Chichester, England, 2001.
- [9] Seracino, R.; Rashid, R.S.M. e Oehlers, D.J., *Generic IC debonding resistances of EB and NSM plates*, Journal of Composites for Construction, ASCE, 2005.
- [10] Matthys, S., *Structural behaviour and design of concrete members strengthened with externally bonded FRP reinforcement*. Thesis in Fulfillment of the requirements for the Degree of Doctor of Applied Sciences, option Structural Engineering, Ghent University, Faculty of Applied Sciences Department of Structural Engineering, Academic year 1999-2000.
- [11] fib bulletin 14, *Externally bonded FRP reinforcement for RC structures*, Technical Report, 2001.
- [12] Marreiros, R., *Degradação da aderência entre CFRP e betão armado devida a envelhecimento acelerado*, Dissertation to obtain the Master degree in Civil Engineering – Engineering of Structures orientation, Instituto Superior Técnico, Universidade Técnica de Lisboa, 2005.
- [13] Rodrigues, C.M.C., *Comportamento da ligação aço-resina-betão em elementos estruturais*, Dissertation to obtain the Master degree in Civil Engineering – Engineering of Structures orientation, Instituto Superior Técnico, Universidade Técnica de Lisboa, 1993.
- [14] Biscaia, H.E.C. and Silva, Manuel A.G., *Environmental effects on bond of GFRP external reinforcement to RC beams*, FRPRCS-8 University of Patras, Greece, July 16-18, 2007.
- [15] Cervenka, V.; Jendele, L. and Cervenka, J., *ATENA - Program documentation, Part 1: Theory*, September, 2006.
- [16] Täljsten, B., *Plate Bonding – Strengthening of existing concrete structures with epoxy bonded plates of steel or fiber reinforced plastics*, Doctoral Thesis, Division of Structural Engineering, Lulea University of Technology, ISSN 0348-8373, Sweden, 1994.